Nucleic Acids Research, 2005, Vol. 33, No. 10 ***3245–3252***
doi:10.1093/nar/gki629

Visualizing the dynamic behavior of poliovirus plus-strand RNA in living host cells

Zong-Qiang Cui[1,3], Zhi-Ping Zhang[1], Xian-En Zhang[1,2,*], Ji-Kai Wen[1], Ya-Feng Zhou[1] and Wei-Hong Xie[1]

[1]State Key Laboratory of Virology, Wuhan Institute of Virology, Chinese Academy of Sciences, Wuhan 430071, China, [2]State Key Laboratory of Biomacromolecules, Institute of Biophysics, Chinese Academy of Sciences, Beijing 100101, China and [3]Graduate School, Chinese Academy Sciences, Beijing 100039, China

Received February 16, 2005; Revised April 28, 2005; Accepted May 14, 2005

ABSTRACT

Dynamic analysis of viral nucleic acids in host cells is important for understanding virus–host interaction. By labeling endogenous RNA with molecular beacon, we have realized the direct visualization of viral nucleic acids in living host cells and have studied the dynamic behavior of poliovirus plus-strand RNA. Poliovirus plus-strand RNA was observed to display different distribution patterns in living Vero cells at different post-infection time points. Real-time imaging suggested that the translocation of poliovirus plus-strand RNA is a characteristic rearrangement process requiring intact microtubule network of host cells. Confocal-FRAP measurements showed that 49.4 ± 3.2% of the poliovirus plus-strand RNA molecules diffused freely (with a *D*-value of $9.6 \pm 1.6 \times 10^{-10}$ cm^2/s) within their distribution region, while the remaining (50.5 ± 2.9%) were almost immobile and moved very slowly only with change of the RNA distribution region. Under the electron microscope, it was found that virus-induced membrane rearrangement is microtubule-associated in poliovirus-infected Vero cells. These results reveal an entrapment and diffusion mechanism for the movement of poliovirus plus-strand RNA in living mammalian cells, and demonstrate that the mechanism is mainly associated with microtubules and virus-induced membrane structures.

INTRODUCTION

Intracellular viral nucleic acids monitoring is of great importance for understanding the virus–host interaction. One of the interests in this aspect is to monitor the localization and movement of the viral nucleic acids in host cells (1–3). So far, a methodology for such a purpose has still been a big challenge, especially for elucidating the dynamic mechanisms of the viral nucleic acids in living host cells (4). Fluorescence *in situ* hybridization (FISH) is a highly efficient method to localize the specific DNA/RNA in cells and thus has been widely used. However, fixation procedures as described in FISH protocols are not compatible with imaging DNA or RNA molecules in living cells (4,5). An alternative means is to microinject radio or fluorescence-labeled RNA/DNA into living cells to study intracellular RNA/DNA localizations and kinetics (6–8). In this way, however, the modification of RNA/DNA of interest and the denaturation of their linking protein are inevitable in the synthesis and extraction procedures, making it difficult to ensure that the observed patterns truly reflect the behaviors of endogenous RNA/DNA in living cells. It is well known that synthesized nucleic acids *in vitro* do not necessarily have the same characteristic as the native viral nucleic acids. Fluorescently labeled linear oligonucleotide probes complementary to target RNAs were used for the detection of endogenous RNA in living cells (9–12), but this method could not be widely used due to the difficulty in separating the hybridization signals from the fluorescence of free probes. RNA-binding proteins fused to GFP were used to tag endogenous RNA in living cells (2,13–15). For instance, the protocol based on the system that synchronously expressed MS2-GFP fusion protein and the reporter RNA containing tandemly repeated MS2 binding sites was widely used to study the characters of endogenous RNA (13–15). However, some of the expressed GFP-fusion proteins may not bind to the RNA of interest. If the RNA has a big sequence like the coronaviral genome, it will be a complicated and burdensome task to build a report system. In this article, by introducing 'molecular beacons' into virus-infected living cells, we built a universal and straight-forward approach for directly visualizing the dynamic behavior of single-strand viral RNA/DNA in its native environment.

*To whom correspondence should be addressed. Tel: +86 10 58881508; Fax: +86 10 58881559; Email: Zhangxe@mail.most.gov.cn

Molecular beacon is a kind of stem–loop oligonucleotide probe that has a fluorescent dye at one end and a quencher moiety at the opposite end (16,17). When there is a target DNA/RNA, the loop sequence hybridizes with the complementary sequence to open the stem, which separates the fluorophore from the quencher, emitting fluorescence. When there is no target sequence, molecular beacon is non-fluorescent in a closed stem–loop conformation. Because of its ultrahigh sensitivity, superior specificity, the possibility to detect without separation, high signal-to-background ratio, and wide temperature range to hybridize to targets, molecular beacon is becoming a leading oligonucleotide probe in a variety of applications (16–18). These include *in vitro* DNA/DNA and DNA/RNA hybridization assays, protein/DNA interactions, as well as in real-time detection and visualization of RNA in living cells (19–25). Here, we used a molecular beacon as the detection probe for real-time visualization of the poliovirus (pv) plus-strand RNA in its host cells.

Poliovirus is a single plus-strand RNA virus. After the entry of pv genomic RNA into a host cell, a polyprotein is translated and subsequently processed into function proteins of which protein 2B, 2C and 2BC can induce membrane vesiculation and rearrangement (26–28). Plus-strand genomic RNA is copied by the viral 3D polymerase into minus-strand RNA, which acts as a template for the synthesis of progeny plus-strands in the multi-strand replicative intermediate (RI) in a rosette-like arrangement of several vesicles (28–30). In virus-infected cells, both plus- and minus-strand RNA synthesis are associated with specific cellular membranous structures, which may provide an efficient replication environment. Around peak RNA synthesis, viral RNAs and RNA-associated membranous structures migrate to the cell center to form a characteristic juxtanuclear area of vesicles (2,26). Although many studies have focused on pv replication and its host cell alterations following infection, the dynamic characters of pv RNA in live cells and its control mechanism remain undetermined. In this work, we imaged the dynamic behavior of pv plus-strand RNA in real-time, and proposed an entrapment and diffusion mechanism for its localization and movement in living host cells.

MATERIALS AND METHODS

Preparation of virus-infected cells

Vero (African green monkey kidney) cells cultured in 35 mm glass bottom culture dishes were infected with poliovirus 1 strain Sabin1 (kindly provided by professor Hu Yunzhang, Institute of Medical Biology, Chinese Academy of Medical Sciences, Kunming 650107) at a multiplicity of infection of 30 p.f.u. The virus was allowed to adsorb for 30 min at 4°C. After one wash with serum-free medium, cells were incubated in RPMI 1640 medium containing 2% fetal calf serum (FCS) (Gibco) at 35°C in 5% CO_2 and used for transfection experiments at various times post-infection (p.i.). To disrupt microtubules, the cells were incubated with a medium containing 20 μM colcemid (Sigma) for 1 h before transfection experiments. To disrupt microfilaments, the cells were incubated with a medium containing 50 nM swinholide (Sigma) for 2 h before transfection experiments.

Design and synthesis of probes

Probes were designed based on genome sequence and structure of poliovirus 1 strain sabin1 (AY184219, NCBI) (31,32), by using RNAdraw, primer premier 5.0 and NCBI BLAST. Probes specific to pv plus-strand RNA were synthesized and purified by TaKaRa Biotech Co., Ltd. (Dalian, China). Three probes (MB: TAMRA-GCGACCAGAATGGCATACCGCC-CTTGAGTCGC-DABCYL; P_2: TAMRA-GCGACCAGAA-TGGCATACCGCCCTTGAGTCGC; P_3: FITC-GACGCTG-ATGTATCCGCCTTCGGTGAAACTAT) were mainly used in the current study.

Fluorescence *in situ* hybridization

Poliovirus-infected Vero cells in dishes were fixed with 4% paraformaldehyde in 1× phosphate-buffered saline (PBS; 10 mM Na_2HPO_4, 1 mM KH_2PO_4, 137 mM NaCl and 3 mM KCL, pH 7.4) at room temperature for 30 min. Then removed the paraformaldehyde and after two washes with 1× PBS, cells were hybridized at 37°C for about 4 h in 1× PBS buffer containing 400 nM of probes. Cells were washed and maintained in 1× PBS buffer for imaging under confocal microscope with a 543 or 488 nm excitation beam.

Delivery of probes into living cells

The probes were delivered into living cells using the TransFast™ transfection reagent (Promega, E2431, USA) as described previously (20). In brief, a transfection mixture, containing 9 μg of transfast™ reagent and 2 μg of the probe dissolved in 0.8 ml of HEPES buffer (145 mM NaCl, 5 mM KCl, 1 mM $MgCl_2$, 1 mM $CaCl_2$, 10 mM glucose and 10 mM HEPES, pH 7.4), was prepared and incubated at room temperature for 10–15 min, and then added to cells after removing the growth medium. Following incubation at 35°C for 40–50 min, the transfection mixture was removed and fresh RPMI 1640 medium containing 2% FCS was added. Culture dishes were placed onto the incubator of the confocal microscope for observation.

Image acquisition and data collection

Except for the electron microscopy (EM) experiments, all imaging experiments were made using a TCS SP2 Leica laser scanning spectral confocal microscope equipped with a cooled CCD camera. For living cell imaging, the prepared cell culture dishes were placed in a temperature-controlled incubator at 35°C and detection was made using a 63× oil objective (NA 1.32) with a 543 nm excitation beam. FRAP (fluorescence recovery after photobleaching) experiments were carried out with the standard Leica confocal microscope and the Lica FRAP software (the advanced time-lapse software). The diffusion coefficients (*D*-values) were calculated as described in (33–35). To measure the *D*-values of the pv plus-strand RNA in aqueous solution, FRAP experiments were made in RNA/MB hybridization solution that was made with 20 nM MB and excessive pv RNA in 2.5 μl HEPES buffer, and sandwiched between two coverslips to form 5 μm-thick aqueous layers. The pv plus-strand RNA was extracted from pv concentrated with PEG 6000 by Trizol (Invitrogen). Unless indicated, all imaging experiments were performed at 35°C in a temperature-controlled incubator equipped on the confocal microscope. For EM, cells were fixed with 2.5%

glutaraldehyde–2% OsO_4, and embedded in Spurr resin by standard protocols. The EM sections were observed in a HITACHI H-7000 FA electron microscope.

RESULTS

FISH in pv-infected cells

To test whether the designed MB can be specifically hybridized to the target viral RNA in pv-infected cells, FISH experiments were performed by using MB and probe P_3 targeting against a different region of the pv plus-strand RNA. Figure 1 shows the TAMRA-labeled MB and FITC-labeled probe P_3 could be co-localized in fixed pv-infected Vero cells at 3 h p.i. Compared with the low fluorescence background of the probe MB in non-pv infection Vero cells (Figure 1A), specific fluorescent signals of pv plus-strand RNA could be detected by using MB (Figure 1B) and P_3 (Figure 1C) in pv-infected cells, although confusion fluorescence could be occasionally seen in cell nuclei. The co-localization of probe MB and P_3 in pv-infected Vero cells (Figure 1D) indicated that the MB could be specifically hybridized to pv plus-strand RNA in pv-infected cells.

Visualizing poliovirus plus-strand RNA in living Vero cells

To visualize pv plus-strand RNA in living cells, MB was transfected into pv-infected Vero cells by liposome at various times p.i. Forty to fifty minutes after the addition of liposome-carried MB, there was fluorescence inside living pv-infected Vero cells. As shown in Figure 2B–D, MB-target hybridization fluorescence signals that represented pv plus-strand RNAs appeared only in the cytoplasm and accumulated in small, irregularly sized granules in the cytoplasm, which is the characteristic display of pv RNA in host cells as described previously (3). Non-pv-infection Vero cells showed little fluorescence 40–50 min after the addition of liposome-carried MB (Figure 2A), and still had very low fluorescence 1.5 h after they were transfected with MB. A molecular beacon designed specifically for porcine parvovirus genomic DNA was also introduced into pv-infected Vero cells, and showed no apparent fluorescence within the first 1 h of the probe uptake (data not shown). When liposome-carried probe P_2 without the quencher was added into non-pv-infection Vero cells, the fluorescence intensity increased constantly during the first 40–50 min, and then became approximately a plateau. The probe P_2 was found to be distributed in the nuclei of living Vero cells (Figure 2F and G), which meant that MB molecules in non-infected cells and the excessive MB in pv-infected cells were both distributed in cell nuclei, although showing no fluorescent signals (Figure 2A). Many articles reported that oligonucleotides can be rapidly taken up by the nucleus although the mechanism is not well understood (6). These experiments also ensured that the fluorescent signals in the cytoplasm of pv-infected cells really came from the hybridization of RNA-MB, and were not caused by the degradation of MB.

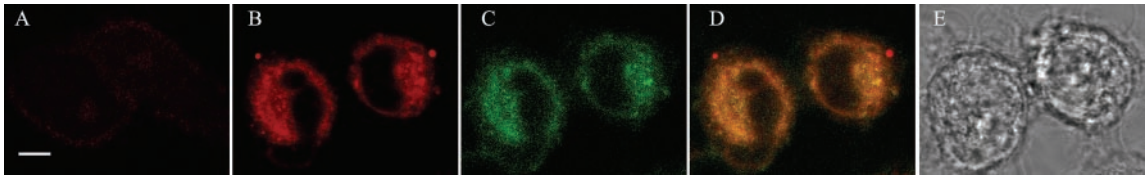

Figure 1. Co-localization of MB and P_3 in pv-infected Vero cells by FISH. (**A**) The low fluorescence background of the MB in non-pv-infection cells. (**B** and **C**) The fluorescence of TAMRA-labeled MB (**B**) and that of FITC-labeled P_3 (**C**) in the same fixed pv-infected Vero cells at 3 h p.i. (**D**) The co-localization of MB and P_3 in the fixed pv-infected Vero cells. (**E**) The phase-contrast image of the cells in images (B–D). Bar, 8 μm.

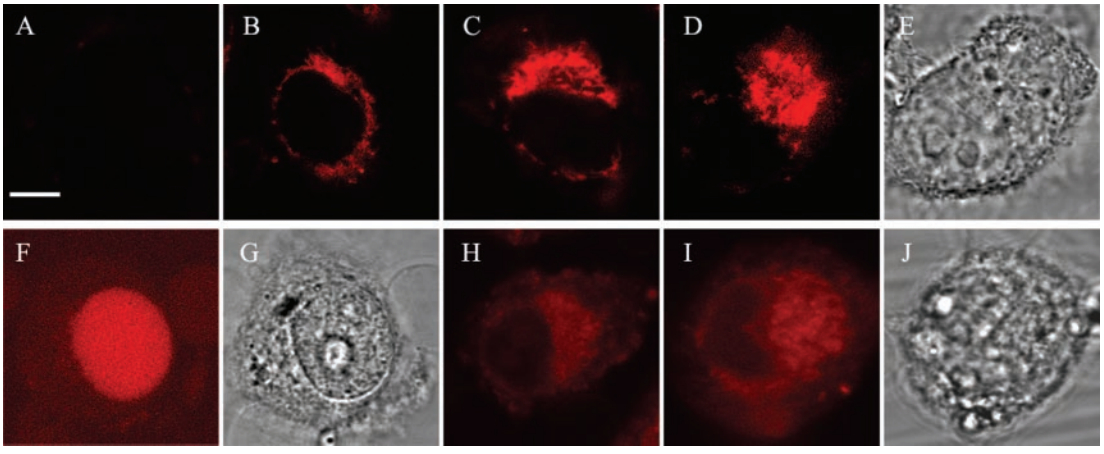

Figure 2. Visualizing pv plus-strand RNA in living pv-infected Vero cells. (**A**) Control non-infection Vero cell shows no obvious fluorescence after being transfected with molecular beacons. (**B**–**D**) Pv plus-strand RNA, detected with a TAMRA-labeled molecular beacon transfected into living cells at different time p.i., was found dispersed in the cytoplasm around the nucleus in small granules at 1 h p.i. (B) and migrated to one side of the cells at 2.5 h p.i. (C) and mainly concentrated in juxtanuclear area at 4 h p.i. (D). (**E**) The phase-contrast image of the cell in image (D). (**F** and **G**) Probe P_2 (molecular beacon without the quencher) distributed in nucleus in non-infection Vero cells. (**H** and **I**) Pv plus-strand RNA was detected in fixed pv-infected Vero cells by FISH with the probe P_2 at 2.5 h p.i. (H) and 4 h p.i. (I). (**J**) The phase-contrast image of the cell in image I. Bar, 8 μm.

At different post-infection time points, the fluorescence signals of MB-RNA hybridization were observed to display different distribution patterns in living Vero cells. At 1 h p.i., the granules of RNA localized in perinuclear area of the cytoplasm (Figure 2B). As the time passed, the RNA granules manifold and most of them appeared on one side of the cell adjacent to the nucleus (Figure 2C). At 4 h p.i., the signals of pv plus-strand mainly concentrated in a nearly circular, juxtanuclear area (Figure 2D and E). As controls, FISH experiments were performed in parallel in fixed Vero cells 1.5 h after infection and the same results could be obtained (Figure 2H–J), confirming that living cell studies truly display the localization of viral RNA in host cells.

It was found that, within the viral RNA distribution region in pv-infected Vero cells, there was often an empty area in which little fluorescent signal was seen during 2–3 h p.i. This phenomenon might display a special procedure during the course of pv RNA replication and transport in host cells. Figure 3 shows a series of selected optical sections of such a cell along the *z*-axis by confocal microscopy (spacing 0.8 μm) at 2.75 h p.i. By using this technique, we can make the 3D-reconstruction of the living cell, which may help us to understand more clearly and accurately the distribution and localization of signals in living cells.

Real-time imaging showed that the translocation of pv plus-strand RNA is a characteristic rearrangement procedure

Distribution change with time implied there should be a translocation process for pv plus-strand RNA in pv-infected cells. Visualization of RNA in living cells enabled us to monitor the transport and movement of viral RNA in real-time. Figure 4 shows a series of selected time-lapse images of a pv-infected Vero cell from 2 to 3 h p.i. The results clearly displayed the translocation process of pv plus-strand RNA in living host cells and substantiated the ordered procedure in real-time. The signals of pv RNA distributed in the perinuclear area at 2 h p.i., moved along with time and formed a juxtanuclear distribution region at about 3 h p.i. As it is similar to pv-induced membrane rearrangement process, this RNA translocation pattern was also defined as rearrangement. Since the pattern can be observed in many pv-infected Vero cells, it is considered that the translocation of pv plus-strand RNA is a programmed and characteristic RNA rearrangement procedure in pv-infected Vero cells.

The translocation and rearrangement of poliovirus plus-strand RNA requires an intact microtubule network

Cytoskeletons have been proved to play an important role in RNA's localization and movement in mammalian cells and in yeast (13–15,22). Their functions include compartmentalizing specific RNA in its region, anchoring static particles, providing track for directional motion and long distance transport, and so on. To examine whether cytoskeletons are also active in the translocation and rearrangement of pv plus-strand RNA in pv-infected cells, microtubules and microfilaments were disrupted by colcemid and swinholide, respectively, in pv-infected Vero cells. Destruction of microtubules had a strong effect on the translocation pattern of pv plus-strand RNA. After pv-infected cells were treated with 20 μM colcemid for an hour, pv plus-strand RNA dispersed either in the perinuclear area or throughout the cytoplasm of host Vero cells (Figure 5A and D), which was a different distribution pattern from that in normal pv-infected cells (Figure 5B and E), and could no longer migrate to form a round, juxtanuclear area of distribution. Destruction of microfilaments with swinholide did not change the distribution (Figure 5C and F) and translocation of pv plus-strand RNA obviously. These results indicate that microtubules play a crucial role in the translocation and rearrangement of pv plus-strand RNA in host cells. In other words, pv can utilize microtubules of the host cell to entrap and transport its RNAs to a destination where they can function.

Dynamic characters of poliovirus plus-strand RNA inside its distribution region uncovered by Confocal-FRAP measurements

Time-lapse images disclosed the characteristic rearrangement process of pv plus-strand RNA in living cells. It is a relatively

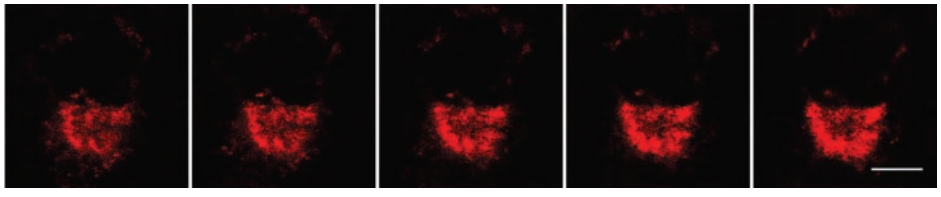

Figure 3. Visualization of pv plus-strand RNA in a series of optical sections through a living pv-infected cell at 2.75 h p.i., spaced 0.8 μm apart. A central area of the distribution region of pv plus-strand RNA was left free from the fluorescence signal. Bar, 8 μm.

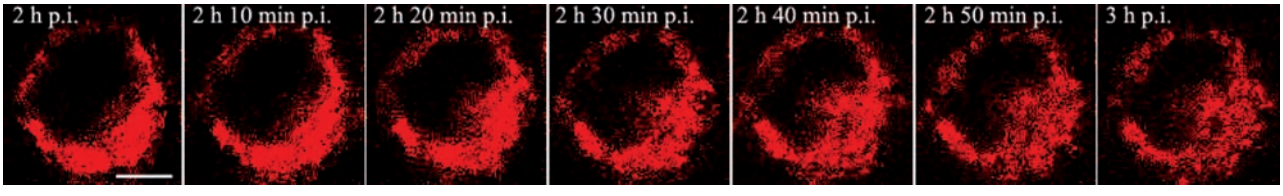

Figure 4. Real-time observation of the translocation of pv plus-strand RNA by using the TAMRA-labeled molecular beacon in a pv-infected Vero cell from 2 to 3 h p.i. Images were acquired every 2 min over a period of 60 min by using Lica time-lapse acquisition software. Bar, 8 μm.

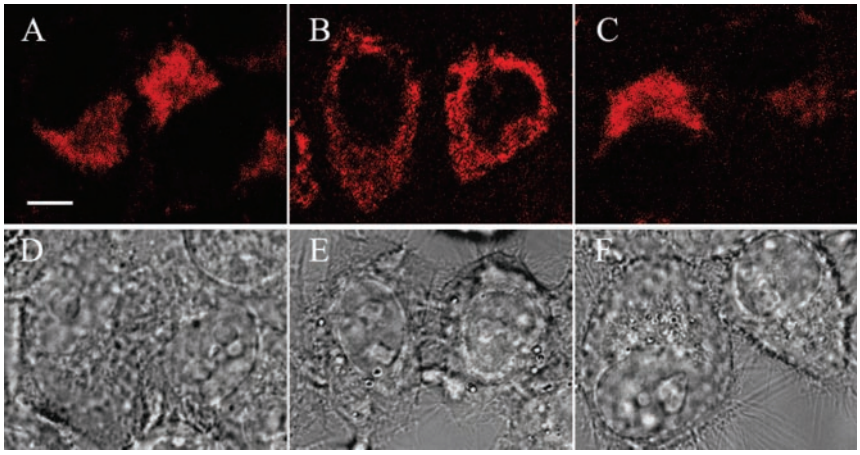

Figure 5. Destruction of microtubules altered the distribution pattern of pv plus-strand RNA in host cells. (**A**) Pv plus-strand RNA concentrated near one side of the cell nucleus in pv-infected Vero cells with intact microtubules at 3 h p.i. (**B**) Pv plus-strand RNA dispersed throughout the cytoplasm in the microtubule-disrupted Vero cell. (**C**) Destruction of microfilaments with swinholide did not change the distribution of pv plus-strand RNA. (**D–F**) are the corresponding phase-contrast images to (A–C), respectively. Bar, 8 μm.

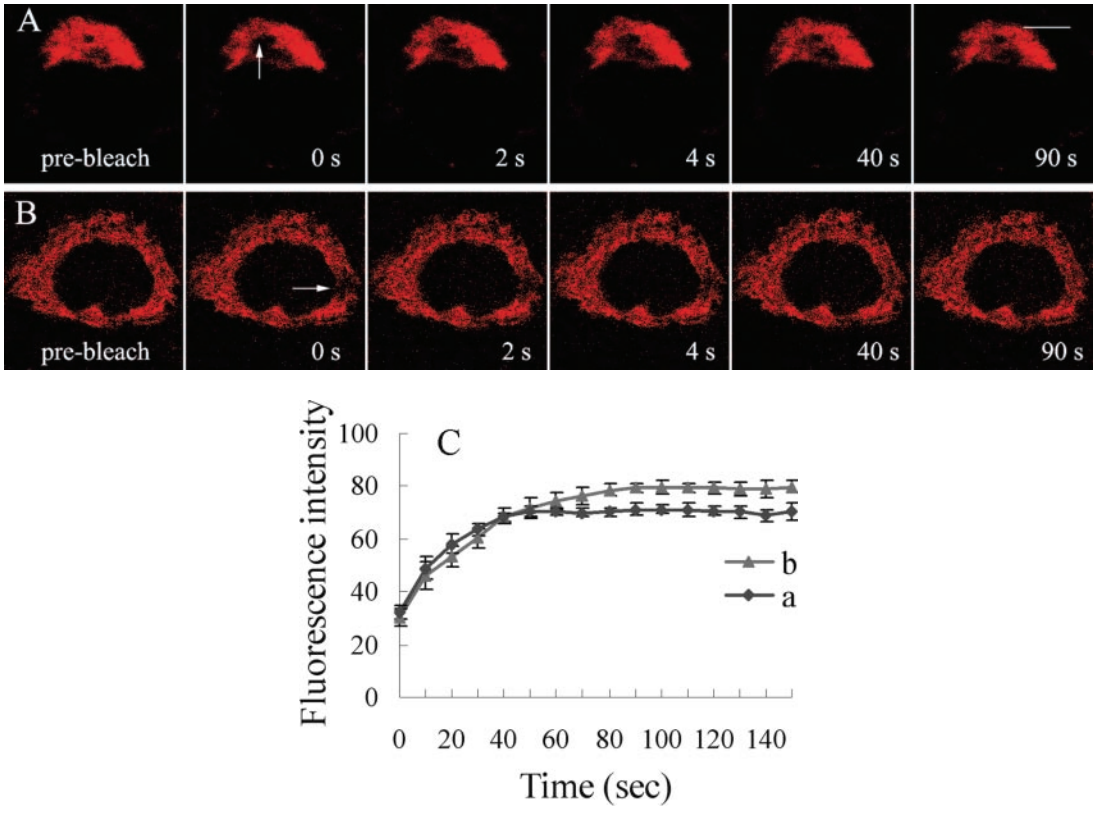

Figure 6. Diffusion dynamics of pv plus-strand RNA as revealed by FRAP in normal pv-infected Vero cell and in the microtubule-disrupted Vero cell. Confocal-FRAP measurements were carried out in pv-infected Vero cells using a 63× objective at 3 h p.i. (**A**) Serial FRAP images in a normal pv-infected Vero cell. (**B**) Serial FRAP images in a pv-infected Vero cell treated by 20 μM colcemid for 1 h. (**C**) Typical recovery curves ($n = 7$) of the FRAP measurements in normal pv-infected Vero cells (a) and in microtubule-disrupted Vero cells (b). The bleach area was indicated by the arrowhead. Bar, 8 μm.

slow procedure. However, the state for RNA molecules inside its distribution region was still unclear. Did they move very slowly only with the change of the whole distribution region, fixedly anchoring on microtubules? Confocal-FRAP experiments were introduced to answer this question. FRAP is a non-destructive technique that can yield dependable and reproducible results in diffusion measurements of fluorophores and macromolecules in aqueous solutions and living cells (33–35). During the first 10–15 min after removing liposome-MB mixture from cell dishes, FRAP experiments were performed in living host cells with or without chemical treatment, and a few images of typical acquisitions are presented in Figure 6A and B. Measurements in solution were also made as controls. After the mean intensity of the ROIs were recorded and

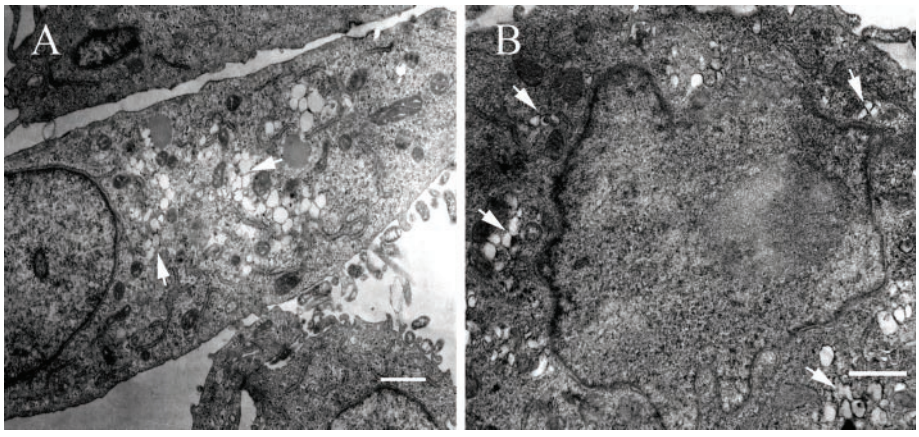

Figure 7. Electron micrographs showed that disruption of microtubules altered the distribution mode of pv-specific membranous vesicle structures (arrowheads) in Vero cells. (**A**) Pv-specific membranous vesicles mainly concentrated in a juxtanuclear area of the intact pv-infected Vero cell at 3.5 h p.i. (**B**) In the microtubule-disrupted pv-infected Vero cell, pv-specific membranous vesicles dispersed throughout the cytoplasm at 3.5 h p.i. Bar, 1 μm.

quantified for a series of FRAP images, recovery curves averaged from seven repeats were drifted, and the mobile fractions and diffusion coefficients were calculated (Figure 6C). The results showed that 49.4 ± 3.2% (n = 7) of RNA molecules could diffuse freely with a diffusion coefficient value of $9.6 \pm 1.6 \times 10^{-10}$ cm^2/s (n = 7) in the distribution region in pv-infected cells while the remaining 50.5 ± 2.9% (n = 7) of RNAs appeared almost static over the measurement time. The diffusion coefficient of the mobile fraction was essentially unchanged at 25°C, which confirmed that the movement was due to diffusion. We also determined that pv plus-RNA diffuses with a rate of $2.8 \pm 0.4 \times 10^{-8}$ cm^2/s in homogeneous aqueous solution.

Considering the alteration in distribution pattern of pv RNA in Vero cells treated with colcemid and the reports that microtubule destruction increased the mobile fraction several times in mammalian cells (15), we had imagined that the mobile fraction of pv plus-strand RNA should also increase greatly and behave in a similar manner after microtubules were destroyed. But it was not the case. In Vero cells that microtubules were disrupted, there were still 39.7 ± 2.4% (n = 5) of pv plus-strand RNAs remaining immobile, which meant the anchor of pv plus-strand RNA was associated not only with microtubules of the host cell, but also with other cell structures considered to be membrane structures as proved elsewhere (3,29,30). Of the 60.4 ± 2.6% (n = 5) that diffused, about 48.1 ± 1.9% RNA molecules had the same diffusion coefficient as in normal pv-infected Vero cells and the other 13.3 ± 1.4% diffused at a lower velocity ($3.7 \pm 0.3 \times 10^{-10}$ cm^2/s). Combining these results with known facts that the RNA replication system of pv was membrane-associated (28–30,36), we supposed that the localization and transport of pv RNA should be controlled by a complex mechanism that mainly involved microtubules and virus-induced membrane structures.

Virus-induced membrane rearrangement is also microtubule-associated in pv-infected Vero cells

The translocation pattern of pv plus-strand RNA molecules obtained in living host cells is similar to the rearrangement mode of pv-induced membranous vesicle structures (27,37). Pv-specific membranous vesicle structures were depicted ~40 years ago (26). Many studies since then have demonstrated the proliferation and rearrangement pattern of these virus-induced vesicular structures in pv-infected cells, and have verified that these membranous vesicle structures were involved in the replication of pv RNA (26–30). Similar to the report of Bolten *et al*. (3), our observations with EM in parallel with RNA detection in living cells suggest that the small pv-specific vesicle clusters correspond to the granules of pv plus-strand RNA. But so far, the mechanism of this pv-specific membrane vesicular translocation and rearrangement is still unclear. We thought that the microtubule network might also play a role in the migration and rearrangement of the pv-specific vesicular structures because destruction of microtubule network altered the RNA distribution and transport pattern. The results from EM (Figure 7) supported this deduction. Starting from ~2 h p.i., in pv-infected cells with intact microtubules, the virus-induced vesicles began to migrate to the inner of the cytoplasm and accumulated in a juxtanuclear area at 3.5 h p.i. (Figure 7A). However, in pv-infected Vero cells in which microtubules were disrupted, pv-induced vesicles did not accumulate with time, but dispersed randomly in the whole cytoplasm at 3.5 h p.i. (Figure 7B). These results showed that the virus-induced membrane rearrangement in pv-infected cells, at least to some degree, was microtubule-dependent.

DISCUSSION

Elucidating the dynamic characters (trafficking routines, velocities, mechanisms, etc.) of viral nucleic acids in host cells is crucial for understanding virus–host interaction. In this report, by introducing MB into living pv-infected Vero cells, we successfully observed the dynamic behaviors of pv plus-strand RNA. Findings in our study indicate that the target-specific molecular beacon is a powerful tool to light RNAs of interest in living cells. As intracellular degradation of molecular beacon remains a problem, the current investigation was mainly focused on the initial phase of probe uptake by cells within 1 h to ensure the reliability of the results (20). With this strategy, the pv plus-strand RNAs were clearly highlighted and their dynamic behaviors were studied in living host cells.

Since pv plus-strand RNA can be directly and specifically lighted by MBs in living cells, its translocation process could be tracked in real-time. To be mentioned, the RNAs displayed in the time-lapse images were the viral RNAs that had already been synthesized before MB was introduced into the cells, and the newly synthesized viral RNAs could no longer be highlighted during the tracking procedure due to the shortage of free MB in the cytoplasm (see Figure 2F and G). However, the RNAs detected at different post-infection time points (Figure 2B–D) were the total pv plus-strand RNAs at the given time. These two experiments displayed similar RNA distribution patterns, indicating that the RNA rearrangement process in Figure 4 represents the change of the distribution region for the total pv plus-strand RNAs at the given time. It has been well documented that the genome replication of pv requires the virus-induced membrane rearrangement (36,38), and that viral progeny plus-strand RNAs are present on the surface of the rosette of pv-specific membrane vesicles (30). Other studies (3) and electron microscopy observations showed that pv plus-strand RNA molecules and pv-induced membranous vesicles had similar distribution patterns, suggesting that the granules of pv plus-strand RNAs correspond to pv-specific membrane vesicle clusters. These findings together suggest that the newly synthesized and the parental pv RNAs have the same distribution region confined by the virus-induced membrane vesicular structures at any given time, and the region changes in accordance with the course of membrane rearrangement. In other words, the pattern of plus-strand RNA translocation and rearrangement represents the membrane rearrangement course in pv-infected cells.

After cell microtubules were disrupted, the translocation and distribution pattern of pv plus-strand RNA were altered, indicating that in addition to pv-induced membrane structures, microtubules also play an important role in the localization and transport of pv RNAs within the host cells. However, pv plus-strand RNAs may not anchor on the microtubules directly as do some other RNAs (15), since disruption of the microtubule network only released a small fraction of the static RNAs (12–15%) and there were still ~40% of plus-strand RNAs remaining almost immobile during the FRAP measurement period. We did not know what the real structure was for the 12–15% mobile RNA fraction additionally released by the destruction of microtubules. This portion of plus-strand RNAs had a lower diffusion velocity than the mobile RNAs in intact pv-infected Vero cells. A possible explanation is that the destruction of microtubules destroyed some of the membrane vesicle structures and caused the release of a kind of unit combined with the plus-strand RNA (39), although we could not exclude the possibility that there might be a small fraction of RNAs combined with specific proteins directly anchoring on the microtubules.

Confocal-FRAP measurements revealed that ~50% of pv plus-strand RNAs diffused freely within their distribution area. The diffusion coefficient ($\sim 9.6 \times 10^{-10}$ cm^2/s) for this fraction of pv plus-strand RNAs in the cytoplasm of Vero cells was similar to the *D*-value (1×10^{-9} cm^2/s) of a portion of cytoplasmic β-actin mRNA labeled by MS2-GFP fusion protein (15). *In vitro* experiment showed that the *D*-value in solution (2.8×10^{-8} cm^2/s) for pv plus-strand RNAs hybridized to molecular beacons was consistent with the literature data for the same size RNAs or DNAs (9,40). In contrast, Lukacs *et al*. reported that the mobility of microinjected DNAs was size-dependent in cytoplasm and nucleus, and the diffusion of DNAs of 3000 bp (double strands) or greater was immeasurably slow (40). These divergent observations may reflect that RNAs behave differently from DNAs in live cells. Indeed, Politz *et al*. found that some poly(A) RNAs diffused freely in the nucleus of cultured rat myoblasts with diffusion rates nearly similar to that in aqueous solutions (9).

Data from EM showed that pv-specific membrane rearrangement requires the intact microtubule network. Pv infection results in profound changes in cellular architecture and morphology, including structural alteration of microtubule-associated proteins (37,41). Our results, together with the phenomenon of cytoskeleton rearrangement observed in pv-infected and other virus-infected cells (37,42), suggest that membrane rearrangement in pv-infected cells is likely associated with microtubule rearrangement.

In conclusion, by using MB and live cell imaging, we have successfully realized the viral nucleic acid detection in living mammalian cells, and have studied the dynamics of pv plus-strand RNA. The work reveals a complex entrapment and diffusion mechanism for the localization and mobility of pv plus-strand RNA in living host cells, and demonstrates that such a mechanism is mainly associated with microtubules and virus-induced membrane structures. Our data also suggest that the interaction between microtubules and membranes plays an important role in the virus-induced membrane rearrangement in pv-infected cells.

ACKNOWLEDGEMENTS

This work was supported by grant KSCXZ-SW-219 from Chinese Academy of Sciences (CAS). Funding to pay the Open Access publication charges for this article was provided by CAS.

Conflict of interest statement. None declared.

REFERENCES

1. Cros,J.F. and Palese,P. (2003) Trafficking of viral genomic RNA into and out of the nucleus: influenza, Thogoto and Borna disease viruses. *Virus Res*., **95**, 3–12.
2. Mcdonald,D., Vodicka,M.A., Lucero,G., Svitkins,T.M., Borisy,G.G., Emerman,M. and Hope,T.J. (2002) Visualization of the intracellular behavior of HIV in living cells. *J. Cell. Biol*., **159**, 441–452.
3. Bolten,R., Egger,D., Gosert,R., Schaub,G., Landmann,L. and Bienz,K. (1998) Intracellular localization of poliovirus plus- and minus-strand RNA visualized by strand-specific fluorescent *in situ* hybridization. *J. Virol*., **72**, 8578–8585.
4. Dirks,R.W., Molenaar,C. and Tanke,H.J. (2001) Methods for visualizing RNA processing and transport pathways in living cells. *Histochem. Cell Biol*., **115**, 3–11.
5. Levsky,J.M. and Singer,R.H. (2003) Fluorescence *in situ* hybridization: past, present and future. *J. Cell Sci*., **116**, 2833–2838.
6. Leonetti,J.P., Mechti,N., Degols,G., Gagnor,C. and Lebleu,B. (1991) Intracellular distribution of microinjected antisense oligonucleotides. *Proc. Natl Acad. Sci. USA*, **88**, 2702–2706.
7. Ainger,K., Avossa,D., Morgan,F., Hill,S.J., Barry,C., Barbarese,E. and Carson,J.H. (1993) Transport and localization of exogenous myelin basic protein mRNA microinjected into oligodendrocytes. *J. Cell Biol*., **123**, 431–441.

8. Glotzer,J.B., Saffrich,R., Glotzer,M. and Ephrussi,A. (1997) Cytoplasmic flows localize injected oskar RNA in Drosophila oocytes. *Curr. Biol.*, **7**, 326–337.
9. Politz,J., Browne,E., Wolf,D. and Pederson,T. (1998) Intra-nuclear diffusion and hybridization state of oligonucleotides measured by fluorescence correlation spectroscopy in living cells. *Proc. Natl Acad. Sci. USA*, **95**, 6043–6048.
10. Politz,J., Tuft,R., Pederson,T. and Singer,R. (1999) Movement of nuclear poly(A) RNA throughout the interchromatin space in living cells. *Curr. Biol.*, **9**, 285–291.
11. Molenaar,C., Marras,S.A., Slats,J.C.M., Truffert,J.-C., Lemaitre,M., Raap,A.K., Dirks,R.W. and Tanke,H.J. (2001) Linear 2′-*O*-Methyl RNA probes for the visualization of RNA in living cells. *Nucleic Acids Res.*, **29**, e89.
12. Tsuji,A., Koshimoto,H., Sato,Y., Hirano,M., Sei-Iida,Y., Kondo,S. and Ishibashi,K. (2000) Direct observation of specific messenger RNA in a single living cell under a fluorescence microscope. *Biophys. J.*, **78**, 3260–3274.
13. Bertrand,E., Chartrand,P., Schaefer,M., Shenoy,S., Singer,R. and Long,R. (1998) Localization of ASH1 mRNA particles in living yeast. *Mol. Cell*, **2**, 437–445.
14. Forrest,K.M. and Gavis,E.R. (2003) Live imaging of endogenous RNA reveals a diffusion and entrapment mechanism for *nanos* mRNA localization in *Drosophila*. *Curr. Biol.*, **13**, 1159–1168.
15. Fusco,D., Accornero,N., Lavoie,B., Shenoy,S.M., Blanchard,J.-M., Singer,R.H. and Bertrand,E. (2003) Single mRNA molecules demonstrate probabilistic movement in living mammalian cells. *Curr. Biol.*, **13**, 161–167.
16. Tyagi,S. and Kramer,F.R. (1996) Molecular beacons: probes that fluoresce upon hybridization. *Nat. Biotechnol.*, **14**, 303–308.
17. Tyagi,S., Bratu,D.P. and Kramer,F.R. (1998) Multicolor molecular beacons for allele discrimination. *Nat. Biotechnol.*, **16**, 49–53.
18. Tsourkas,A., Behlke,M.A., Rose,S.D. and Bao,G. (2003) Hybridization kinetics and thermodynamics of molecular beacons. *Nucleic Acids Res.*, **31**, 1319–1330.
19. Sokol,D.L., Zhang,X., Lu,P. and Gewirtz,A.M. (1998) Real time detection of DNA RNA hybridization in living cell. *Proc. Natl Acad. Sci. USA*, **95**, 11538–11543.
20. Matsuo,T. (1998) *In situ* visualization of messenger RNA for basic fibroblast growth factor in living cells. *Biochem. Biophys. Acta.*, **1379**, 178–184.
21. Perlette,J. and Tan,W. (2001) Real-time monitoring of intracellular mRNA hybridization inside single living cells. *Anal. Chem.*, **73**, 5544–5550.
22. Bratu,D.P., Cha,B.J., Mhlanga,M.M., Kramer,F.R. and Tyagi,S. (2003) Visualizing the distribution and transport of mRNAs in living cells. *Proc. Natl Acad. Sci. USA*, **100**, 13308–13313.
23. Nitin,N., Santangelo,P.S., Kim,G., Nie,S. and Bao,G. (2004) Peptide-linked molecular beacons for efficient delivery and rapid mRNA detection in living cells. *Nucleic Acids Res.*, **32**, e58.
24. Santangelo,P.J., Nix,B., Tsourkas,A. and Bao,G. (2004) Dual FRET molecular beacons for mRNA detection in living cells. *Nucleic Acids Res.*, **32**, e57.
25. Tyagi,S. and Alamadi,O. (2004) Imaging native β-actin mRNA in motile fibroblasts. *Biophys. J.*, **87**, 4153–4162.
26. Bienz,K., Egger,D. and Pasamontes,L. (1987) Association of polioviral proteins of the P2 genomic region with the viral replication complex and virus-induced membrane synthesis as visualized by electron microscopic immunocytochemistry and autoradiography. *Virology*, **160**, 220–226.
27. Cho,M.W., Teterina,N., Egger,D., Bienz,K. and Ehrenfeld,E. (1994) Membrane rearrangement and vesicle induction by recombinant poliovirus 2C and 2BC in human cells. *Virology*, **202**, 129–145.
28. Bienz,K., Egger,D., Troxler,M. and Pasamontes,L. (1990) Structural organization of poliovirus RNA replication is mediated by viral proteins of the P2 genomic region. *J. Virol.*, **64**, 1156–1163.
29. Egger,D., Terina,N., Ehrenfeld,E. and Bienz,K. (2000) Formation of the poliovirus replication complex requires coupled viral translation, vesicle production, and viral RNA synthesis. *J. Virol.*, **74**, 6570–6580.
30. Bienz,K., Egger,D., Pfister,T. and Troxler,M. (1992) Structural and functional characterization of the poliovirus replication complex. *J. Virol.*, **66**, 2740–2747.
31. Nomoto,A., Omata,T., Toyoda,H., Kuge,S., Horie,H., Kataoka,Y., Genba,Y., Nakano,Y. and Imura,N. (1982) Complete nucleotide sequence of the attenuated poliovirus Sabin 1 strain genome. *Proc. Natl Acad. Sci. USA*, **79**, 5793–5797.
32. Minor,P.D. (1992) The molecular biology of poliovaccines. *J. Gen. Virol.*, **73**, 3065–3077.
33. Axelrod,D., Koppel,D.E., Schlessinger,J., Elson,E.L. and Webb,W.W. (1976) Mobility measurements by analysis of fluorescence photobleaching recovery kinetics. *Biophys. J.*, **16**, 1055–1089.
34. Handwerger,K.E., Murphy,C. and Gall,J.G. (2003) Steady-state dynamics of Cajal body components in the *Xenopus* germinal vesicle. *J. Cell Biol.*, **160**, 495–504.
35. Klein,C., Pillot,T., Chambaz,J. and Drouet,B. (2003) Determination of plasma membrane fluidity with a fluorescent analogue of sphingomyelin by FRAP measurement using a standard confocal microscope. *Brain Res. Protocols*, **11**, 46–51.
36. Schlegel,A., Giddings,T.H.Jr, Ladinsky,M.S. and Kirkegaard,K. (1996) Cellular origin and ultrastructure of membranes induced during poliovirus infection. *J. Virol.*, **70**, 6576–6588.
37. Lenk,R. and Penman,S. (1979) The cytoskeletal framework and poliovirus metabolism. *Cell*, **16**, 289–301.
38. Schwartz,M., Chen,J., Lee,W.-M., Janda,M. and Ahlquist,P. (2004) Alternate, virus-induced membrane rearrangements support positive-strand RNA virus genome replication. *Proc. Natl Acad. Sci. USA*, **101**, 11263–11268.
39. Egger,D., Pasamontes,L., Bolten,R., Boyko,V. and Bienz,K. (1996) Reversible dissociation of the poliovirus replication complex: functions and interactions of its components in viral RNA synthesis. *J. Virol.*, **70**, 8675–8683.
40. Lukacs,G.L., Haggie,P., Seksek,O., Lechardeur,D., Freedman,N. and Verkman,A.S. (2000) Size-dependent DNA mobility in cytoplasm and nucleus. *J. Biol. Chem.*, **275**, 1625–1629.
41. Joachims,M. and Etchison,D. (1992) Poliovirus infection results in structural alteration of a microtubule-associated protein. *J. Virol.*, **66**, 5797–5804.
42. Pelkmans,L., Puntener,D. and Helenius,A. (2002) Local actin polymerization and dynamin recruitment in SV40-induced internalization of caveolae. *Science*, **296**, 535–539.